Internet Journal of Society for Social Management Systems Vol.12 Issue 2 sms19-1843
ISSN: 2432-552X
ORIGINAL ARTICLE

Fundamental Study on the Correlation between Scaling Resistance and Pore Structure Evaluated using Drilling Powder

Shunsei Tanaka[1*], Yuya Sakai[2]

[1] School of Civil Engineering, The University of Tokyo
4-6-1 Komaba, Muguro-ku, Tokyo, 153-8505, JAPAN

[2] Instisute of Industrial Science, The University of Tokyo
4-6-1 Komaba, Muguro-ku, Tokyo, 153-8505, JAPAN

[*]E-mail: shtanaka@iis.u-tokyo.ac.jp

***Abstract*:** As a fundamental study to establish a method to evaluate the scaling resistance of concrete in a short period based on the analysis of drilling powder, the correlation between the scaling resistance of cementitious materials and the pore structure was evaluated using drilling powder. First, a small-sized sample salt scaling test was performed on mortar specimens for 20 cycles, and scaling dulability index was calculated based on the residual mass. And drilling powder was collected from the specimens prepared under the same conditions immediately before the first freezing-and-thawing cycle starts. Subsequently, the pore structure was investigated using mercury intrusion porosimetry (MIP). When a fine powder is to be investigated using MIP, the large diameter of a pore includes voids between the particles, which is easily disturbed owing to human operation. To exclude these voids, the effective pore size range was determined to be 10 nm to 250 nm by referring to past studies. The drilling powder from the mortar specimen is composed of the powder derived from sand and the powder derived from cement paste at an arbitrary ratio. To evaluate the pore information of the cement paste part, which influences the scaling deterioration, a method that quantifies the volume of cement paste and sand in the drilling powder by performing heating and acid dissolution was proposed. Subsequently, a high correlation was observed between the scaling resistance of the mortar specimen and the pore volume of the cement paste part of the drilling powder. This result revealed that effective pore structure information related to the scaling resistance of the cement-based material remained in the fine drilling powder.

Keywords: scaling, air content, pore structure, drilling powder, mortar, heating, acid dissolution

1. Introduction

Scaling of concrete is one of the major deteriorations caused by repeated freeze-thaw cycles (Valenza and Scherer, 2007b, 2007a). Numerous studies have been conducted in this regard. Accordingly, it was revealed that the scaling resistance increases with a lower water-to-cement ratio (W/C), more entrained independent air, or a finer pore structure (Powers, 1945; Powers and Helmuth, 1953; Verbeck and Klieger, 1957; Beaudoin and

Received: 2019.07.31/ Accepted: 2020.01.28
Internet Journal of Society for Social Management Systems Published Date: 2020.07.20

MacInnis, 1974; Pigeon, Marchand and Pleau, 1996; Chatterji, 2003; Valenza and Scherer, 2007b, 2007a; Oyamada *et al.*, 2011). It is important to incorporate such knowledge into the design of a new structure under an environment where frost damage is expected (Cho, 2007). However, as cast concrete often has lower quality than the designed one owing to construction failure (Feld and Carper, 1996), it is necessary to evaluate the scaling resistance not only at the design stage, but also after the construction is completed or during service to determine and update an effective maintenance plan. Standards such as ASTM C672, RILEM CDF, and JIS A 1148A have been proposed to evaluate the scaling resistance. However, evaluation through these standards requires several months, which is not practically short (Oyamada *et al.*, 2011). Especially in Japan, where an increase in inspection demand and a reduction in inspection staff and budgets is expected in the future, an inspection method that can save time and effort is required.

Studies conducted so far have examined the methods of estimating the strength of cement paste and mortar based on the information obtained from drilling powder (Tanaka and Sakai, 2019b). It was confirmed that the information regarding the pore structure, which dominates the compressive strength of the specimens, remains in fine powder. As it is known that the pore structure is related to the scaling resistance(Wieloch and Klemm, no date; Walker and Hsieh, 1968; Koh and Kamada., 1973; Litvan, 1983; Feldman, 1986; Klemm and Klemm, 1997), it is possible to predict the scaling resistance of concrete based on the analysis of drilling powder. In this method, the only tool needed to be taken to the site is a drill weighing a few kilograms, and the measurement of the pore structure can be done in a few days, which enables to shorten the test period of the scaling resistance. Furthermore, drilling can be performed even with a 1 mm drill (Tanaka and Sakai, 2019a), whose size is equal to or smaller than that of the surface voids of the structures. Therefore, the aesthetic defects and structural damage caused to the structure can be mitigated for inspection. In addition, previous studies have confirmed that it is possible to measure the carbonation depth and chloride ion penetration depth by observing the drill hole (Tanaka and Sakai, 2019a). When it is considered that frost damage becomes serious under the presence of salt, it is favourable that both the scaling resistance and chloride ion penetration depth can be investigated with a single drill hole.

Considering the above background, a basic study was conducted to develop a semi-destructive scaling resistance inspection method that can reduce the amount of work to be performed on the site and shorten the test period. As one of those method, analysis of drilling powder was focused on in this study. Experiment was performed to confirm whether effective information regarding the scaling resistance remained in the fine drilling powder by determining the correlation between the pore structure evaluated using the drilling powder and the scaling resistance of mortar samples.

2. Methodology

2.1 Material properties

Ordinary Portland cement was used as the cement, and crushed sandstone was used as the fine aggregate. The properties of the cement were as follows: density of 3.15 g/cm^3, brain value of 3380 cm^2/g, and ignition loss of 2.58 %. The properties of the fine aggregate were as follows: surface dry density of 2.65 g/cm^3, dry density of 2.62 g/cm^3, ignition loss of 2.31 %, water absorption rate of 1.32 %, and fineness modulus of 3.04.

Table 1 Mortar mix proportions

ID	Parameter	Unit content (kg/m^3)					
	W/C	Cement	Water	Sand	SP*1	TA*2	AFA*3
M30	30	972	292	1060	9	0	0.00
M40	40	836	335	1060	8	0	0.00
M50	50	734	367	1060	0	7	0.07
M60	60	654	392	1060	0	12	0.12
M70	70	590	413	1060	0	12	0.12

*1: Super Plasticizer, *2: Thickening Agent, *3: Anti-forming Agent

Figure 1 Photo of small-sized samples during scaling test

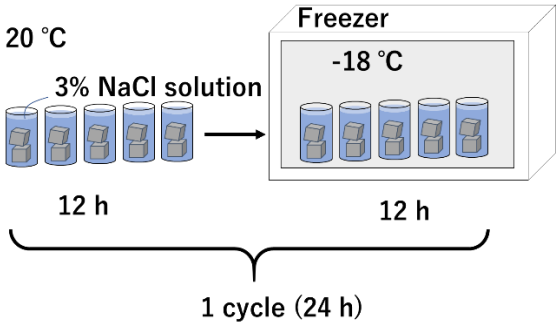

Figure 2 Overview of the freezing-and-thawing cycle

2.2 Experiment on mortar

2.2.1 Specimen preparation

An experiment to determine the correlation between the freezing-thawing resistance and the pore structure of the drilling powder for mortar specimens was conducted.

Table 1 shows the mix proportions of the mortar specimens. Mortar was cast into a steel mould of width 4 cm and length 2 cm to a height of 2 cm. After 24 h, the mould was removed, and the specimen was cut into cubes of side 2 cm with a diamond cutter for small-sized sample salt scaling test (Oyamada *et al.*, 2011; Kanno *et al.*, 2015). Subsequently, the specimens were cured in water for seven days. Note that past studies (Oyamada *et al.*, 2011; Kanno *et al.*, 2015) performed scaling tests using specimens of cubes of side 8 mm, but 2 cm cubic specimens were used in this study because 8 mm cubic samples were too small to perform drilling.

2.2.2 Small-sized salt scaling test on mortar

As shown in Figure 1, two pieces of samples were placed in a 50 mL polypropylene container filled with a NaCl 3 % solution. Subsequently, these samples were subjected to 20 freezing-and-thawing cycles. As illustrated in Figure 2, a single cycle lasted 24 h, which consisted of 12 h in a room at 20 °C and 12 h in a freezer at −18 °C. The scaling was evaluated at

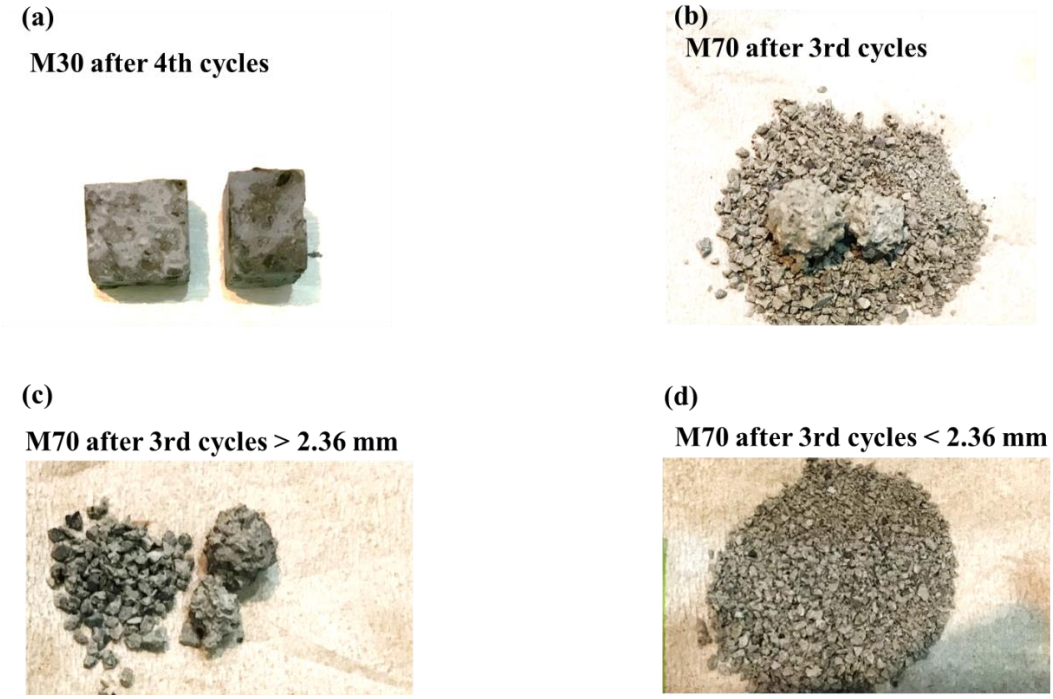

Figure 3 Samples before and after the small-sized sample salt scaling test

the end of the 5th, 10th, 15th, and 20th cycles. Especially, for M60 and M70, scaling was also evaluated at the 3rd and 4th cycles as it progressed radically in these two cases. Figure 3(a) shows a small-sized sample with little scaling and Figure 3(b) shows a sample with some scaling. The evaluation of the scaling is shown below. After a predetermined cycle, the sample was filtered with filter paper and washed with pure water to remove NaCl. The sample was dried at 40 °C for 72 h, and then sorted with a 2.36 mm sieve (Oyamada *et al.*, 2011; Kanno *et al.*, 2015) as shown in Figure 3(c) and (d). The residual mass ratio, which is defined by Eq.(1), was measured.

$$Residual\ mass\ ratio\ = \frac{m_{>2.36}}{m_{all}} \qquad (1)$$

where $m_{>2.36}$ is defined as the mass of the part remaining on the 2.36 mm sieve and m_{all} is defined as the mass of the entire sample.

2.2.3 Mercury intrusion test for drilling powder

After the specimen was cured, drilling powder was collected from one of the specimens by using a drill with a diameter of 2 mm. Immediately after drilling powder was obtained, D-drying was performed for 24 h, and subsequently, drilling powder was placed in a sealed container until pore structure evaluation.

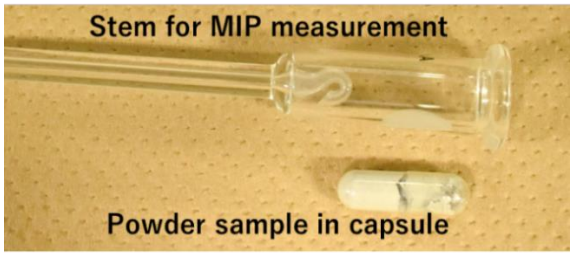

Figure 4 Setup for the pore structure evaluation of powder

The pore structure was evaluated using mercury intrusion porosimetry (MIP). The measured pore size range was 10 nm to 8000 nm. To prevent the powder from being drawn into the MIP apparatus, measurement was performed with the powder in a gelatine capsule as shown in Figure 4.

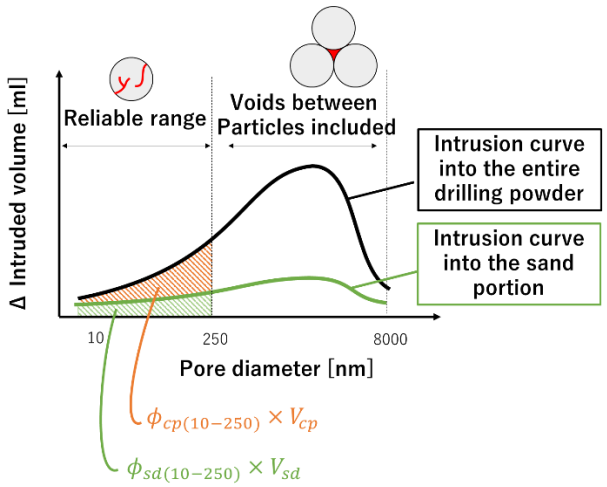

Figure 5 Image of intrusion curve obtained by mercury intrusion test for drilling powder

2.2.4 Evaluation of pore structure from mercury intrusion curve

As illustrated in Figure 5, the mercury intrusion curve obtained for the drilling powder of mortar includes not only intrusion into the pores in the particles but also intrusion into the voids between the particles(Tanaka and Sakai, 2019b). The voids between the particles should be excluded from consideration below because they include a human error regarding how to pack the powder into capsules. As discussed in a previous report (Tanaka and Sakai, 2019b), the size of the void between particles should be considered to be dependent on the particle diameter. This study follows the past report and it is assumed that, in the pore size range of 250 nm or less in the mercury intrusion curve, the intrusion into the voids between particles is small and the intrusion into the pores in the particles is dominant. Hence, only the range from 10 nm to 250 nm is used to evaluate the pore structure in this study.

The drilling powder collected from mortar contains a portion derived from cement paste and a portion derived from sand. As it is believed that the pore in the cement paste portion, which has a porous structure, is dominant in freezing and thawing, the pore volume in the cement paste portion was determined using the following equation from the measurement result of the entire drilling powder:

$$\phi_{cp(10-250)} = \frac{\phi_{all(10-250)} \cdot V_{all} - \phi_{sd(10-250)} \cdot V_{sd}}{Vcp} \quad (2)$$

$$V_{all} = V_{cp} + V_{sd} \quad (3)$$

where $\phi_{cp(10-250)}$, $\phi_{all(10-250)}$, and $\phi_{sd(10-250)}$ are the pore volume for the pore sizes of 10 nm to 250 nm per unit volume of cement paste portion (mL/mL), the pore volume for the pore sizes of 10 nm to 250 nm per unit volume of drilling powder (mL/mL), and the pore volume for the pore sizes of 10 nm to 250 nm per unit volume of sand portion (mL/mL), respectively. $\phi_{sd(10-250)}$ was determined in advance using the preliminary test described in 2.2.5. $V_{all}, V_{sd}, and\ V_{cp}$ represent the volume of the drilling powder used for MIP measurement (mL), the volume of the powder derived from the cement paste portion included in V_{all} (mL), and the volume of the powder derived from the sand portion included in V_{all} (mL).

V_{all}, V_{cp}, and V_{sd} were determined through heating and acid dissolution processes, both of which are described in 2.2.6.

2.2.5 Determination of $\phi_{sd(10-250)}$

The powder of sand was made using a disk mill, and D-drying was performed immediately for 24 h. Subsequently, the pore structure was evaluated using MIP as illustrated in 2.2.3. From this result, $\phi_{sd(10-250)}$ was obtained using the following equation:

$$\phi_{sd(10-250)} = \frac{V_{intr(10-250)}}{V_{sd}0} \quad (4)$$

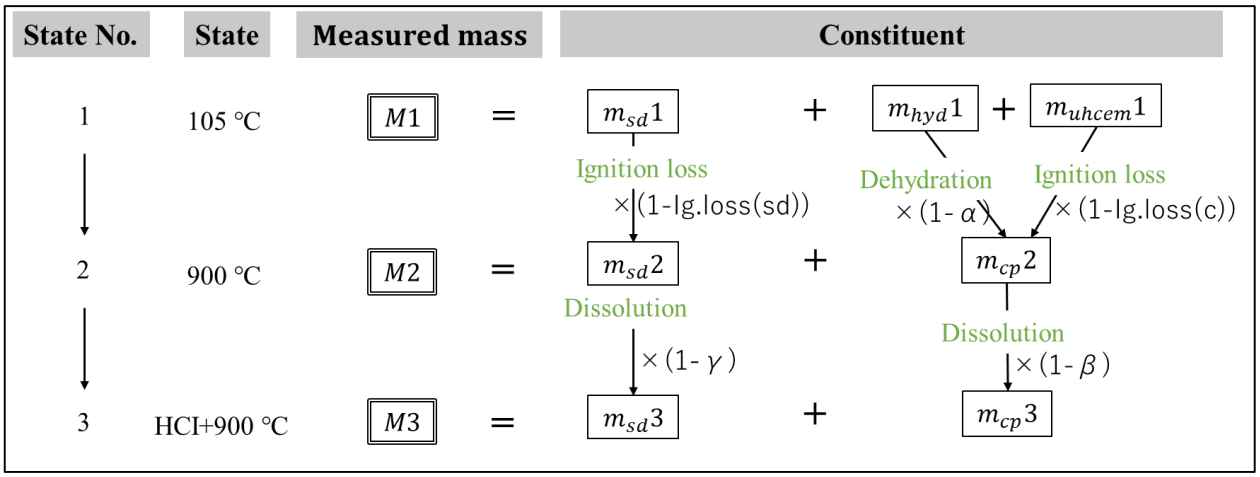

Figure 6 Flow of the heating and acid dissolution processes and mass change during the test

where $V_{intr(10-250)}$ is the mercury volume intruded into pores of size 10 nm to 250 nm, and $V_{sd}0$ is the volume of sand powder used in this preliminary test. $V_{sd}0$ was obtained by dividing the sample mass measured immediately before the MIP measurement by the dry density of the sand (shown in 2.1).

Through this preliminary test, $\phi_{sd(10-250)}$ was determined to be 0.0256 (mL/mL).

2.2.6 Heating and acid dissolution processes

The flow of the heating and acid dissolution processes is shown in Figure 6. First, the drilling powder was heated at 105 °C for 24 h (State 1). *M1* is the sample mass measured after State 1. Second, the sample measured after State 1 was heated at 900 °C for 30 min (State 2). *M2* is the sample mass measured after State 2. Finally, the sample after State 2 was stirred well in HCl (1+100) for 20 min. The amount of HCl was 250 mL per 1 g of powder sample. Subsequently, the remaining part was collected with filter paper and heated at 900 °C for 30 min (State 3). *M3* is the sample mass measured after State 3. $m_{hyd}X$, $m_{uhcem}X$, $m_{sd}X$, and $m_{cp}X$ are the masses of the hydrate portion, unhydrated cement portion, sand portion, and cement paste portion in the drilling powder at State X (X=1, 2, 3), respectively. In Figure 6, the phenomenon that causes mass change between different states is shown in green letters. It is assumed that the hydrate portion in State 1 becomes indistinguishable from the unhydrated cement portion after it is dehydrated in State 2. Hence, the hydrate portion and the unhydrated cement portion in State 1 are expressed together as a component derived from cement paste (cp) in State 2 and State 3.

The following equations can be derived from the diagram in Figure 6:

$$m_{hyd}1 + m_{uhcem}1 + m_{sd}1 = M1 \quad (5)$$

$$m_{cp}2 + m_{sd}2 = M2 \quad (6)$$

$$m_{cp}3 + m_{sd}3 = M3 \quad (7)$$

$$(1 - Ig.loss(c)\{(1-\alpha)m_{hyd}1 + m_{uhcem}1\} = m_{cp}2 \quad (8)$$

where α is the mass reduction ratio of the hydrate from 105 °C to 900 °C and it was set to 0.186 based on a past study (Taylor, 1977). *Ig.loss(c)* is the ignition loss of the unhydrated cement shown in 2.1. It is assumed that dehydrated hydrate has the same ignition loss as the unhydrated cement.

$$(1-\beta)m_{cp}2 = m_{cp}3 \quad (9)$$

where β is the mass reduction ratio before and after the acid dissolution of the powder derived from the cement paste portion, which is determined to be 0.89 through a preliminary test.

$$(1 - Ig.loss(sd))m_{sd}1 = m_{sd}2 \quad (10)$$

where *Ig.loss(sd)* is the ignition loss of sand shown in 2.1.

$$(1 - \gamma)m_{sd}2 = m_{sd}3 \quad (11)$$

where γ is the mass reduction ratio before and after the acid dissolution of the powder derived from the sand portion, which is determined to be 0.054 through a preliminary test.

By solving these equations simultaneously, $m_{hyd}1$, $m_{uhcem}1$, $m_{sd}1$, $m_{cp}2$, $m_{sd}2$, $m_{cp}3$, and $m_{sd}3$ can be calculated. Subsequently, $V_{hyd}1$, $V_{uhcem}1$, and V_{sd} (which correspond to the volumes of the hydrate portion, unhydrated cement portion, and sand portion in the drilling powder, respectively) are obtained by dividing $m_{hyd}1$ by the density of the hydrate, which is defined below, $m_{uhcem}1$ by the density of the cement shown in 2.1, and $m_{sd}1$ by the dry density of the sand shown in 2.1, respectively. For the density of hydrates, a wide range of values has been reported, such as 2.2 g/cm^3 to 2.6 g/cm^3 depending on the preprocess (Jennings, 2008). The determination of the density of the hydrate has scope for further discussion; however, it was set to 2.4 g/cm^3 in this study because it did not affect the interpretation of the following results irrespective of the setting of density between 2.2 g/cm^3 and 2.6 g/cm^3.

Finally, V_{cp} in Eq. (3) is calculated using the following equation:

$$V_{cp} = V_{hyd}1 + V_{uhcem}1 \quad (12)$$

3. Results and discussions

Figure 7 shows the result of a small-sized sample salt scaling test on mortar. The residual mass ratio calculated in Eq.(1) is shown as the average for two small samples placed in the same container. Based on this result, scaling durability index **(**SDI) (Oyamada *et al.*, 2011, 2015), which is an index of scaling resistance and is defined by the equation shown below, was calculated as the quantitative scaling resistance of the specimen.

$$SDI = P \times \frac{N}{M} \quad (13)$$

where M is the number of cycles at which the test ends (= 20 in this case), N is the smaller of the two i.e. the number of cycles when the residual mass ratio becomes below 60 % for the first time or M, and P is

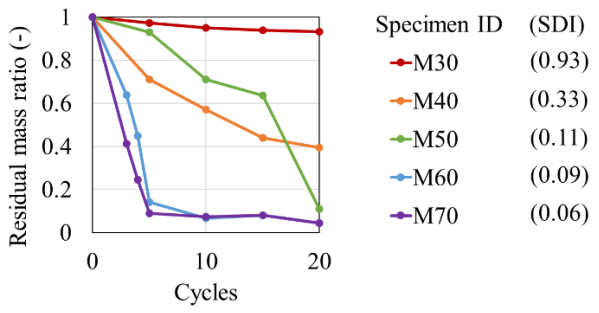

Figure 7 Residual mass ratio change during small-sized sample salt scaling test on mortar

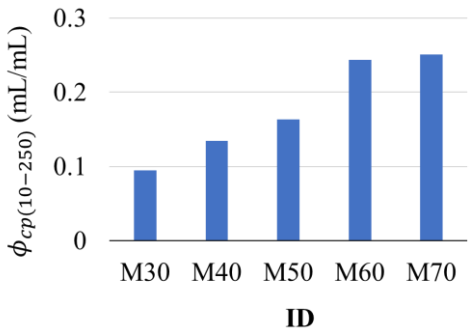

Figure 8 $\phi_{cp(10-250)}$ of mortar calculated using Eq. (2) based on the result of MIP measurement

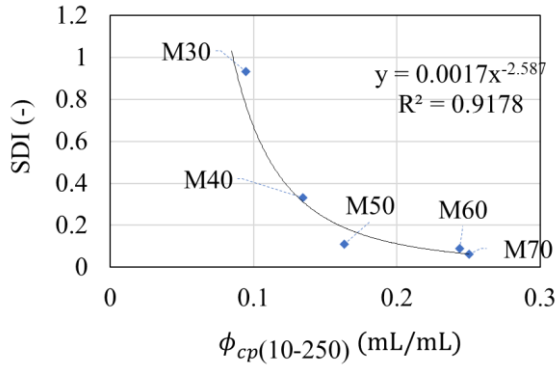

Figure 9 SDI of mortar vs. $\phi_{cp(10-250)}$ of mortar

the residual mass ratio at N cycles.

The values of SDI are shown beside the legend in Figure 7.

Figure 8 shows the result of measurement of $\phi_{cp(10-250)}$ of the mortar samples. $\phi_{cp(10-250)}$ becomes higher with higher W/C, which is consistent with the well-known fact that the capillary pore increases with higher W/C (Powers, 1958). This result supports that the pore structure of the cement paste part in the mortar can be evaluated properly using Eq. (5) to Eq. (13).

Figure 9 shows the SDI of mortar versus $\phi_{cp(10-250)}$ measured using the drilling powder. A high correlation between $\phi_{cp(10-250)}$ and the SDI can be observed in the experiment with mortar. This result indicates that the pore size range that has been reported to be correlated to the scaling resistance in the past studies (Wieloch and Klemm, no date; Walker and Hsieh, 1968; Koh and Kamada., 1973; Litvan, 1983; Feldman, 1986; Klemm and Klemm, 1997) can be evaluated even with fine powder, and that the SDI of cement paste can be estimated from the pore information remaining in the drilling powder.

Note that pore size range of 10 nm to 250 nm, which shows a high correlation with SDI in this study, is not necessarily comparable to the pore size range in past studies that discussed the correlation between pore size and freeze-thaw behaviour. That is because many past studies used a sample of size a few millimetres for MIP measurement, but a powder sample was used in this study, which causes a significant difference in the measurement results. In the mercury intrusion test, the smaller the sample size, the larger is the ratio of the surface area to the volume, so that the probability of mercury being trapped in the ink bottle is reduced, in other words, there is a scale effect such that the intrusion volume per sample volume is increased (Yoshino, Kamada and Katsura, 1996).

4. Conclusion

To confirm whether effective information regarding the scaling resistance remains in the fine drilling powder, the correlation between SDI, which is an index of the scaling resistance of specimens, and the pore structure of the drilling powder of mortar was investigated. As a quantitative index of the pore structure of drilling powder, pore volume for the pore sizes 10 nm to 250 nm, which exclude the voids between particles, is calculated. The following conclusions are drawn.

(1) To calculate the pore volume of the cement paste part $\phi_{cp(10-250)}$ using MIP for the drilling powder from mortar specimen, which is composed of a mixture of sand and cement paste, heating and acid dissolution processes were proposed. A reasonable measurement result that $\phi_{cp(10-250)}$ is larger with higher W/C was obtained.

(2) $\phi_{cp(10-250)}$ and the SDI of the mortar specimen showed a high correlation with a determination coefficient of 0.92. This result indicates that effective pore information related to the scaling resistance of the specimens remains in the pore structure information of the drilling powder of mortar.

References

1) Beaudoin, J. J. and MacInnis, C., 1974. The mechanism of frost damage in hardened cement paste, *Cement and Concrete Research*, 4(2), pp. 139–147. doi: 10.1016/0008-8846(74)90128-8.

2) Chatterji, S., 2003. Freezing of air-entrained cement-based materials and specific actions of air-entraining agents, *Cement and Concrete Composites*, 25(7), pp. 759–765. doi: 10.1016/S0958-9465(02)00099-9.

3) Cho, T., 2007. Prediction of cyclic freeze-thaw damage in concrete structures based on response surface method, *Construction and Building Materials*, 21(12), pp. 2031–2040. doi: 10.1016/j.conbuildmat.2007.04.018.

4) Feld, J. and Carper, K. L., 1996. *Construction failure*. John Wiley & Sons.

5) Feldman, R. F., 1986. Influence of Condensed Silica Fume and Sand/Cement Ratio on Pore Structure and Frost Resistance of Portland Cement Mortars, American Concrete Institute Special Publication, 91, pp. 973–990.

6) Jennings, H. M., 2008. Refinements to colloid model of C-S-H in cement: CM-II, *Cement and Concrete Research*, 38, pp. 275–289. doi: 10.1016/j.cemconres.2007.10.006.

7) Kanno, H. et al., 2015. Relationship Between Existing Freeze-Thaw Test And New Test Method With Small Sized Sample, *Cement Science and Concrete Technology*, 68(1), pp. 419–425.

8) Klemm, A. J. and Klemm, P., 1997. Ice formation in pores in polymer modified concrete - II. The influence of the admixtures on the water to ice transition in cementitious composites subjected to freezing/thawing cycles, *Building and Environment*, 32(3), pp. 199–202. doi: 10.1016/S0360-1323(96)00054-6.

9) Koh, Y. and Kamada., E., 1973. The Influence of pore structure of concrete made with absorptive aggregates on the frost durability of concrete., *"Proceedings RILEM/IUPAC International Symposium on Pore Structure and Properties of Materials*, 11, pp. 45–62.

10) Litvan, G. G., 1983. Air Entrainment in the Presence of Superplasticizers, *ACI Journal Proceedings*, 80(4), pp. 326–331.

11) Oyamada, T. et al., 2011. Study on the new test method for freeze-thaw resistance with de-icing chemicals, *Proceeding of the Japan Concrete Institute*, 33(1), pp. 935–940.

12) Oyamada, T. et al., 2015. Proposal of New Evaluation Method for Salt Scaling of Hardened Mortar and Depression with Magnesium Salt SN : *512 Proposal of New Evaluation Method for Salt Scaling of Hardened Mortar and Depression with Magnesium Salt*, doi: 10.13140/RG.2.1.3131.5284.

13) Pigeon, M., Marchand, J. and Pleau, R., 1996. Frost resistant concrete, *Construction and Building Materials*, 10(5 SPEC. ISS.), pp. 339–348. doi: 10.1016/0950-0618(95)00067-4.

14) Powers, T. C., 1945. A Working Hypothesis for Further Studies of Frost Resistance of Concrete, A*CI Journal Proceedings*, 41(1), pp. 245–272. doi: 10.14359/8684.

15) Powers, T. C., 1958. Structure and Physical

Properties of Hardened Portland Cement Paste, *American Ceramic Society*, 41(1), pp. 1–6.

16) Powers, T. C. and Helmuth, R. A., 1953. Theory Of Volume Changes In Hardened Portland-Cement Paste During Freezing, *Highway Research Board Proceedings*, 32, pp. 285–297.

17) Tanaka, S. and Sakai, Y., 2019a. Development and verification of neutralization depth and chloride ion penetration depth measurement method using fibrescope, *Proceedings of The 5th International Conference in Sustainable Construction Materials and Technologies (SCMT5), London, UK.*

18) Tanaka, S. and Sakai, Y., 2019b. Study on the correlation between compressive strength of hardened cement paste and physical properties of drilling powder, *Proceedings of the Japan Concrete Institute*, 41(1), pp. 1853–1858.

19) Taylor, H. F., 1977. *Cement chemistry*. Thomas Telford.

20) Valenza, J. J. and Scherer, G. W., 2007a. A review of salt scaling: I. Phenomenology, *Cement and Concrete Research*, 37(7), pp. 1007–1021. doi: 10.1016/j.cemconres.2007.03.005.

21) Valenza, J. J. and Scherer, G. W., 2007b. A review of salt scaling: II. Mechanisms, *Cement and Concrete Research*, 37(7), pp. 1022–1034. doi: 10.1016/j.cemconres.2007.03.003.

22) Verbeck, G. J. and Klieger, P., 1957. Studies of "Salt" Scaling of Concrete, *Highway Research Board Bulletin*, (150), pp. 1–13. Available at: http://pubsindex.trb.org/view.aspx?id=101892.

23) Walker, R. D. and Hsieh, T., 1968. Relationship Between Aggregate Pore Characteristics And Durability Of Concrete Exposed To Freezing And Thawing, *Highway Research Record*, (226), pp. 41–49.

24) Wieloch, M. and Klemm, A. J., 2005. The Effects Of Pore Structure Of Air- Entrained Cement-Based Mortars On Freezing And Thawing Deterioration, *Proceedings of the PRoBE Conference, Glasgow Caledonian University, Glasgow, UK. 2005*. pp. 517–526.

25) Yoshino, T., Kamada, E. and Katsura, O., 1996. The Equation Describing Concrete Strength as a Function of Pore Structure, *Concrete Research and Technology*, 7(2), pp. 65–72.